Nuclear Physics A, 571, 4, 667-693. DOI:10.1016/0375-9474(94)90715-3

A MODEL FOR THE $\gamma p \longrightarrow \pi^+\pi^- p$ REACTION.

J. A. Gómez Tejedor and E. Oset

Departamento de Física Teórica and IFIC, Centro Mixto Universidad de Valencia - CSIC—— 46100 Burjassot (Valencia), Spain

Abstract

We have studied the $\gamma p \longrightarrow \pi^+\pi^- p$ reaction using a model which includes $N, \Delta(1232), N^*(1440)$ and $N^*(1520)$ intermediate baryonic states and the $\rho - meson$ as intermediate 2π resonance. The model reproduces fairly well experimental cross sections below $E_\gamma = 800\ MeV$ and invariant mass distributions even at higher energies. One of the interesting findings of the study is that the $\gamma N \longrightarrow N^*(1520) \longrightarrow \Delta\pi$ process is very important and interferes strongly with the dominant Δ Kroll Ruderman term to produce the experimental peak of the cross section. We show that the study of the reaction can provide information on some couplings, concretely the $N^*(1520) \longrightarrow \Delta\pi$. We also find that pion energy distributions for different photon energies, which have not been measured so far, contain very valuable information on the dynamics of the reaction. Finally the analogies and differences with respect to the $\pi N \longrightarrow 2\pi N$ reaction are also discussed.

1 Introduction.

The $\gamma p \longrightarrow \pi^+\pi^- p$ reaction has been studied experimentally in the past [1, 2] and there is abundant information on cross sections and invariant mass distributions for the $\pi\pi$ and πN systems. New improvements in experimental techniques and facilities have reopened the study of this reaction at Mainz [3]. The theoretical developments have run parallel to the experimental fate of the reaction, with just one early model [4] which has not been improved so far. Meanwhile the related reaction $\pi N \longrightarrow \pi\pi N$ has been the object of intense experimental [5, 6, 7] and theoretical study [8, 9, 10, 11]. The model of ref. [10] relies upon the coupling of pions to nucleons and resonances incorporating one point, two point and three point diagrams and N, $\Delta(1232)$, $N^*(1440)$ in the intermediate states. This model, when complemented by terms containing N^* intermediate states relevant at higher energies reproduces remarkably well all the cross sections for the different isospin channels in the energy range covered by the present meson physics facilities of Los Alamos, TRIUMF and PSI [12, 14].

The $\pi N \longrightarrow \pi\pi N$ reaction at low energies has recently attracted attention as a good testing ground of chiral symmetry and chiral perturbation theory [14, 13]. However, the $\gamma N \longrightarrow \pi\pi N$ reaction is still relatively unexplored.

One characteristic feature of the $\pi N \longrightarrow \pi\pi N$ reaction is that it requires a fairly large number of Feynman diagrams to account for it theoretically. This number is of the order of 40 in [10, 12]. Hence, the apparent success of the model of [4] for the $\gamma N \longrightarrow \pi\pi N$ reaction which considers only 5 Feynman diagrams has always been intriguing.

With this reaction becoming a target of new experimental study and in-

teresting medium effects predicted for the $(\gamma, \pi^+\pi^-)$ reaction in nuclei [15], in analogy to those already found for the $(\pi, 2\pi)$ reaction [16, 17], a thorough theoretical study of the $\gamma N \longrightarrow \pi\pi N$ reaction is timely and opportune. We undertake this task here and study the $\gamma p \longrightarrow \pi^+\pi^- p$ reaction in detail.

The model is based on the coupling of photons and pions to nucleons and resonances using effective Lagrangians and thus leading to a set of Feynman diagrams at the tree level. We do not implement unitarity in the final states but make an estimate of possible uncertainties stemming from unitarity corrections.

2 The model.

In a model which contains many terms, as the one presented here, it is important to establish a principle of organization. For this purpose we follow the organization scheme of [8] and classify our diagrams in one point, two points and three points diagrams, according to the number of vertices in the hadron components. Our basic components are pions, nucleons and nucleonic resonances. We consider for the hadronic components N, $\Delta(1232, J^\pi = 3/2^+, I = 3/2)$, $N^*(1440, J^\pi = 1/2^+, I = 1/2)$ and $N^*(1520, J^\pi = 3/2^-, I = 1/2)$. The $N^*(1520)$ has a particularly large coupling to the photons and proves to be an important ingredient, mostly because its interference with the dominant component of the process, the $\gamma N \longrightarrow \Delta\pi$ transition through the gauge Kroll Ruderman term. Higher resonances have a weaker coupling to photons and do not interfere with the dominant term, hence their contribution is small, at least for photon energies below 800 MeV, Mainz energies, where our model

is meant to work. Because of the important coupling of the ρ meson to the two pion system and the $\gamma\pi$ system we have also considered terms involving the ρ meson with the same organizing scheme. These terms are only relevant at high energies but show up clearly in the two pion invariant mass distributions at these energies. With these considerations the basic diagrams which we consider have the structure as shown in fig. 1. In diagrams a) and b) the one point $NN\pi\pi$ coupling stands for the s-wave πN interaction. We consider there only the isoscalar part of the amplitude. The isovector part is mediated by ρ exchange [18] and hence it is explicitly taken into account in diagrams f-i. Diagram c) contains the gauge term $NN\pi\gamma$ or Kroll Ruderman term. We use a pseudovector coupling for the $NN\pi$ vertex and this allows us to consider exclusively positive energy intermediate state in the hadronic propagators [19]. In the two point and three point diagrams we include nucleon and the resonances as intermediate states. However, while all possible diagrams with N and Δ intermediate states are considered, we omit some with $N^*(1440)$ intermediate states which are very small. For the $N^*(1520)$ intermediate states we keep only the term which interferes with the dominant term of the amplitude (Δ Kroll Ruderman term). In addition, all different time orderings of the diagrams are considered.

The diagram g) involves a gauge term $\rho\pi\pi\gamma$ coming from minimal coupling in the $\rho\pi\pi$ vertex which contains a derivative coupling. Finally diagram j) contains the anomalous coupling $\gamma 3\pi$ [20].

The Feynman diagrams considered appear in fig. 2. The corresponding amplitudes can be evaluated from the interaction Lagrangians which we show in appendix A. This is easily accomplished by following the Feynman rules

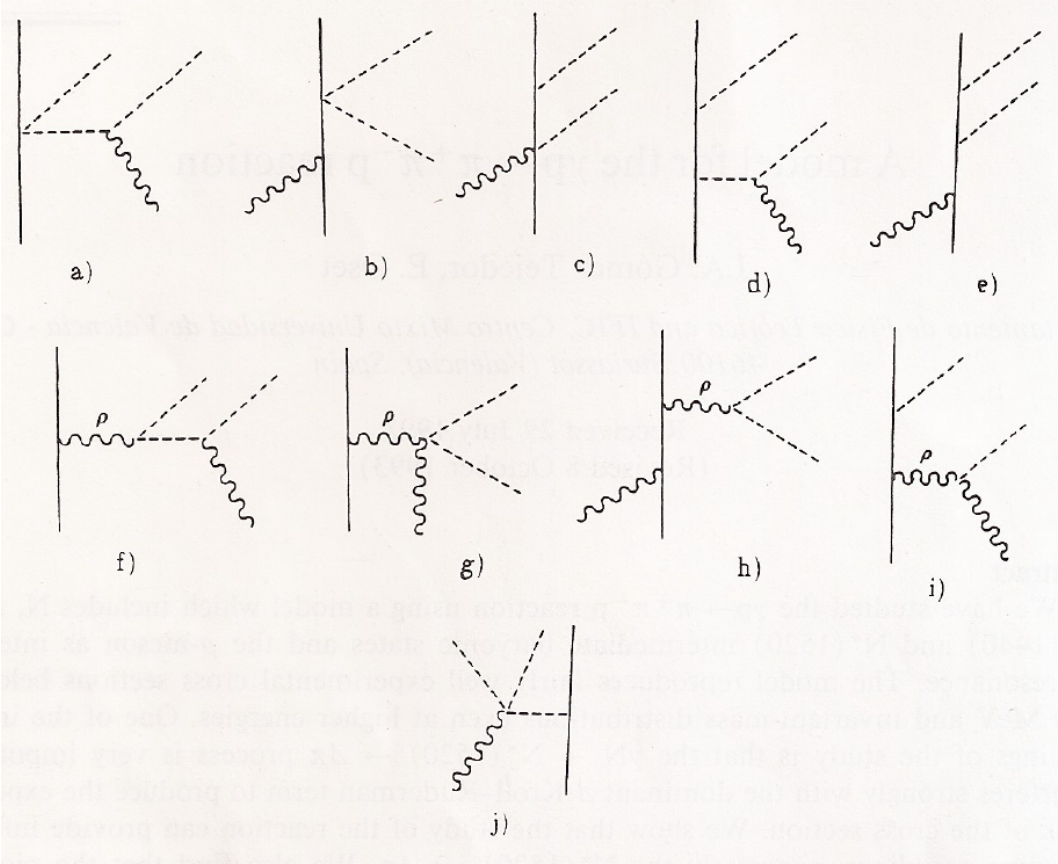

Figure 1: Classification of the Feynman diagrams into one point, two point and three point diagrams.

which are shown in appendix B. From there the amplitudes corresponding to the diagrams of fig. 2 are straightforwardly calculated. Detailed expressions for the amplitudes can be seen in [21].

Most of the interaction Lagrangians in Appendix A are standard. Some of them require an explanation on how they are obtained. The $\Delta N\pi\gamma$ contact term (A.12), or Δ Kroll Ruderman term, is obtained by minimal coupling from the $\Delta N\pi$ Lagrangian (A.3). The $\Delta N^*\pi$ coupling (A.7) has the same structure as the $\Delta N\pi$. The coupling constant is determined from the decay width $N^* \longrightarrow \Delta\pi$ [25]. For the $N^*N\pi$ vertex we take a coupling similar to the non relativistic limit of $NN\pi$ lagrangian (A.1), and the coupling constant is calculate from the $N^* \longrightarrow N\pi$ decay [25]. The couplings $N^*N\gamma$ and $N'^*N\gamma$ (N'^* stands for the $N^*(1520)$ from now on) are obtained in such a way as to reproduce the empirical N^* and N'^* decay helicity amplitudes in the $N\gamma$ channel [25]. The contact term $NN\pi\gamma$ (A.11) is obtained from the pseudovector $NN\pi$ coupling (A.1) by minimal coupling. For the $\Delta N\gamma$ coupling (A.14) we take the coupling constant in agreement with the value obtained by adjusting the $M1^+(3/2)$ amplitude to experiment [19, 22].

The $\Delta\Delta\pi$ coupling (A.4) is not well known empirically. Here we take the results from the quark model with SU(6) symmetry [8, 23], $f_\Delta/f = 4/5$. For the vertex $\Delta\Delta\gamma$ we write directly the vertex contribution to the Feynman rules in (B.10) [31] in analogy to (B.9) for the $NN\gamma$. The magnetic moment of the Δ, μ_Δ, can be calculated in the quark model [26] with the result $\mu_\Delta/\mu_p = e_\Delta/e$. However, we shall use for the Δ^{++} the experimental result based on the πp bremsstrahlung ($\pi^+ p \longrightarrow \pi^+ p\gamma$) [27], $\mu_{\Delta^{++}} = 1.62 \pm 0.18$ (in μ_p units). The contact term $NN^*\pi\gamma$ (A.13) is obtained from the $NN^*\pi$ Lagrangian (A.5)

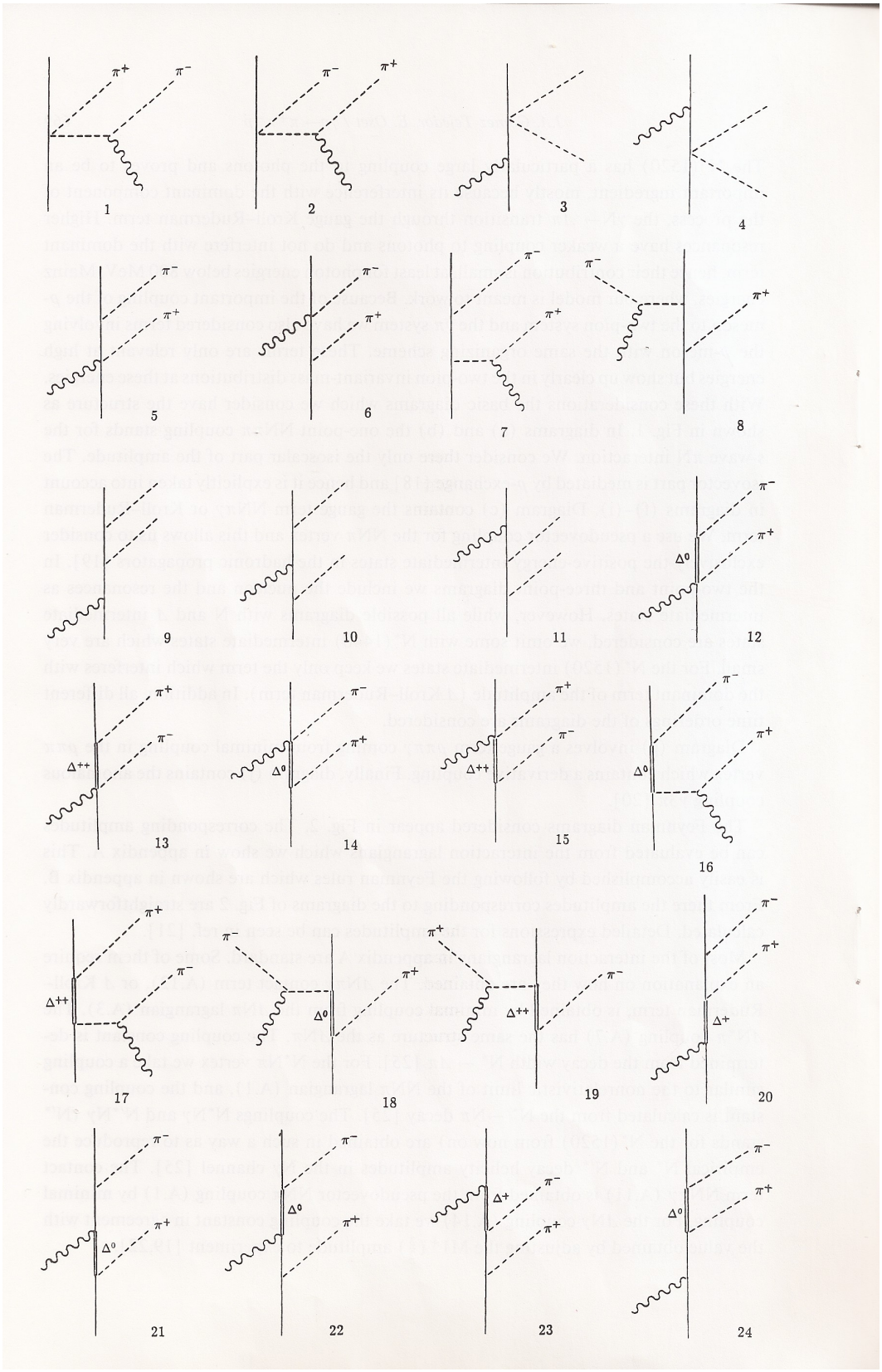
π+
π−
1
π−
π+
2
3
4
π−
π+
5
π−
π+
6
π−
π+
7
π−
π+
8
9
10
11
π−
π+
Δ0
12
π+
π−
Δ++
13
π−
π+
Δ0
14
π+
π−
Δ++
15
π−
π+
Δ0
16
π+
π−
Δ++
17
π−
π+
Δ0
18
π+
π−
Δ++
19
π−
π+
Δ+
20
π−
Δ0
π+
21
π−
Δ0
π+
22
Δ+
π−
π+
23
π−
π+
Δ0
24

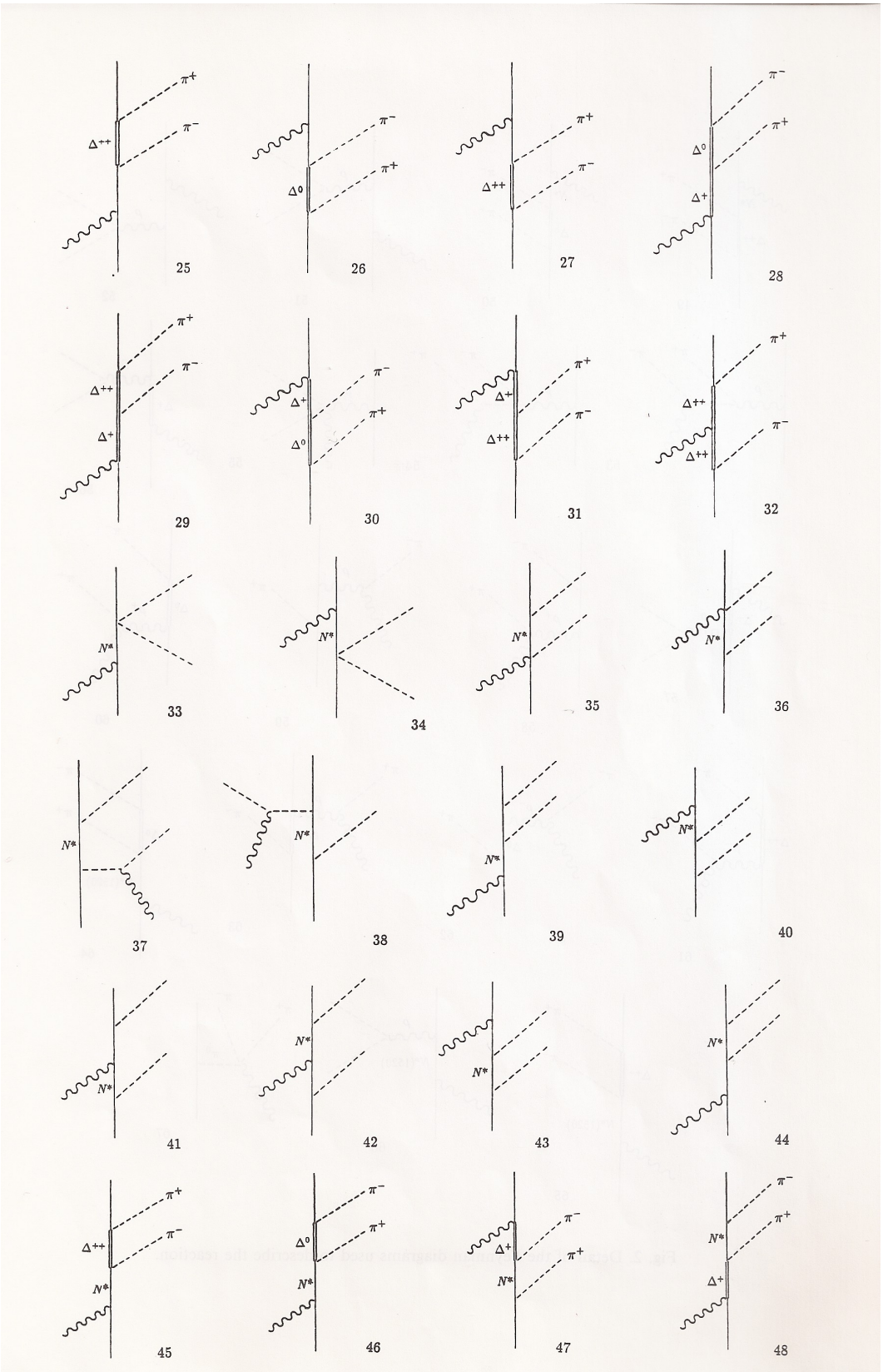
π+
Δ++
π−
25
π−
Δ0
π+
26
π+
Δ++
π−
27
π−
Δ0
π+
Δ+
28
π+
Δ++
π−
Δ+
29
π−
Δ+
π+
Δ0
30
π+
Δ+
Δ++
π−
31
π+
Δ++
π−
Δ++
32
N*
33
N*
34
N*
35
N*
36
N*
37
N*
38
N*
39
N*
40
N*
41
N*
42
N*
43
N*
44
π+
Δ++
π−
N*
45
π−
Δ0
π+
N*
46
π−
Δ+
π+
N*
47
π−
N*
π+
Δ+
48

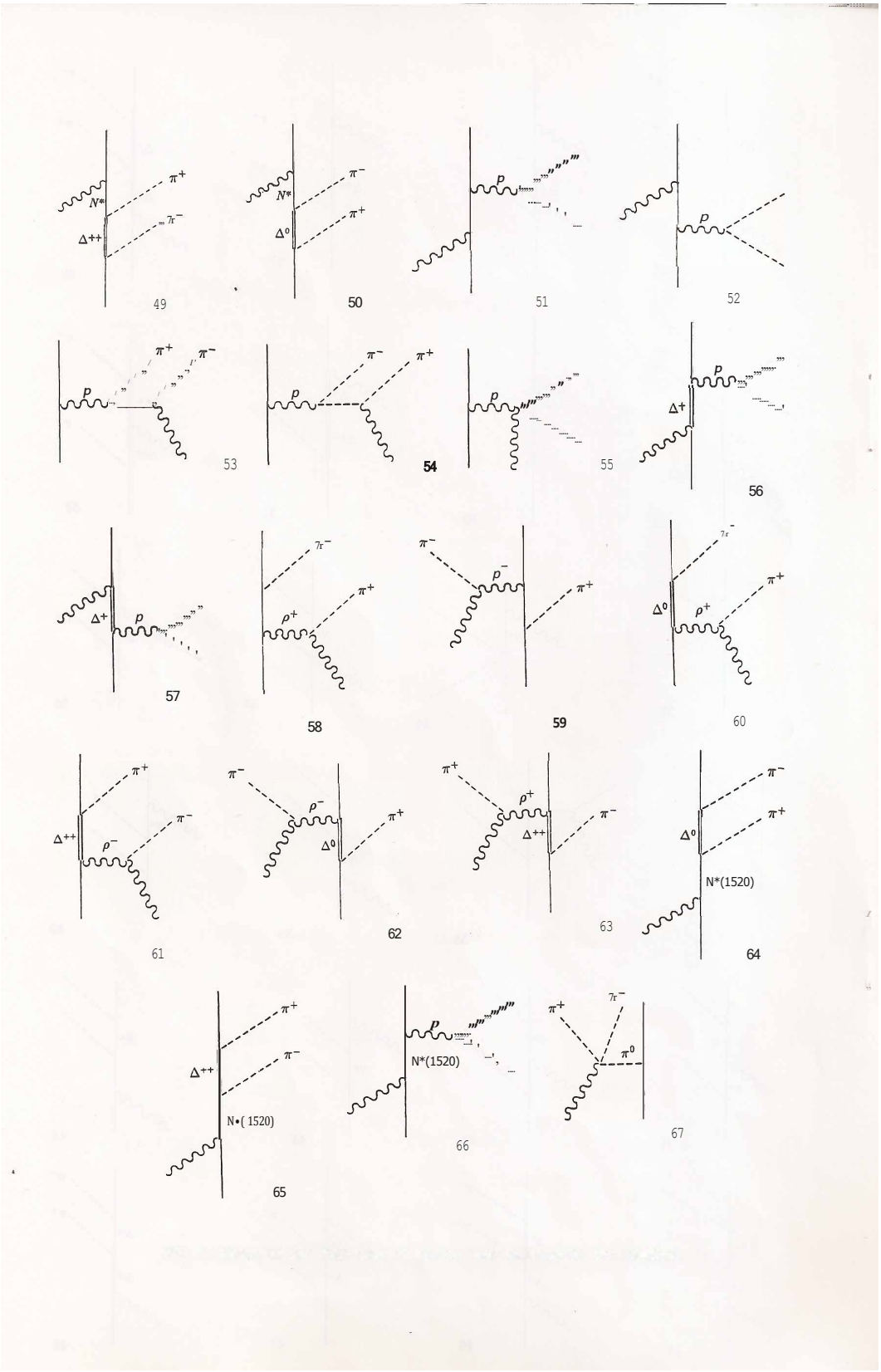

Figure 2: Detail of the Feynman diagrams used to describe the reaction.

by minimal coupling. The term $NN^*\pi\pi$ is taken from [10] and is meant to account for $N^* \longrightarrow N\pi\pi\,(s-state)$. The coupling constant C is corrected with respect to [10] to correct for some rough approximation in the estimation of the width in [10] plus the large changes in the N^* width experienced from the latest edition of the particle data tables [25] to the earliest one [28]. In all cases for the width and ratios of decay we take the average values from the results of [25].

For the $\Delta N'^*\pi$ coupling we have taken the simplest Lagrangian (A.8), compatible with the conservation laws (parity, isospin, rotation invariance, etc.). The transition $N'^* \longrightarrow \Delta\pi$ is $3/2^- \longrightarrow 3/2^+$ in spin and $1/2 \longrightarrow 3/2$ in isospin and a pion of negative intrinsic parity is produced. The strength is fixed from the data of [25]. The sign however is chosen as to have constructive interference. With the chosen sign the agreement with the data is relatively good while with the opposite sign the discrepancies are of about a factor of two and the qualitative features of the experiment are not reproduced.

The ρ coupling constants to N or Δ are scaled from the π couplings with the constant $\sqrt{C\rho}$. With the value $C_\rho = 2$ used here and in [10] one obtains standard ρ coupling to N an Δ used in [10]. However, for the $N'^*N\rho$ vertex (A.20) we take the coupling constant from the decay width $N'^* \longrightarrow N\rho$ [25]. Finally we have also used the $\gamma \longrightarrow 3\pi$ term [20] (A.23) which is related to the anomalous term responsible for $\pi^0 \longrightarrow \gamma\gamma$ decay [29, 30] (A.24), with $F^{3\pi} = F^\pi/ef_\pi^2$ ($f_\pi = 93\,MeV$).

In order to obtain the couplings in appendix B non relativistic approximations have been done in some Lagrangians, but keeping terms up to p/2m and neglecting terms of $(p/2m)^2$ or higher order terms.

Finally one remark about the couplings. Those involving moments in the vertex $\vec{S}\cdot\vec{q}$, etc. are meant to be calculated in the CM of the π, ρ baryon system when they are on shell. In a few cases (when the photon enters the diagram after the pions) the CM frame is ill defined and the vertex is left untouched with the momenta being those appearing in the γp CM frame. These latter terms provide a negligible contribution in our case and consideration of further recoil corrections are unnecessary.

The information provided above, with the one of appendices A, B completes the information about our model. In the following chapters we discuss the relevance of the different terms and the results. The calculations have been performed by evaluating the 67 matrix elements using the Pauli matrix algebra numerically.

3 Results and discussion.

3.1 Total cross section.

The cross section for the $\gamma p \longrightarrow \pi^+\pi^- p$ reaction is given by

$$\sigma = \frac{m}{\lambda^{1/2}(s,0,m^2)} \frac{1}{(2\pi)^5} \int \frac{d^3p_4}{2\omega_4} \int \frac{d^3p_5}{2\omega_5} \int d^3p_2 \frac{m}{E_2}$$

$$\delta^4(k+p_1-p_2-p_4-p_5) \overline{\sum_{s_i}} \sum_{s_f} |T|^2 \tag{1}$$

$$= \frac{m^2}{\lambda^{1/2}(s,0,m^2)} \frac{1}{4(2\pi)^4} \int d\omega_5 d\omega_4 d\cos\theta_5 d\phi_{45}$$

$$\theta(1-cos^2\theta_{45}) \overline{\sum_{s_i}} \sum_{s_f} |T|^2 \tag{2}$$

Where $k = (\omega, \vec{k})$, $p_1 = (E_1, \vec{p}_1)$, $p_2 = (E_2, \vec{p}_2)$, $p_4 = (\omega_4, \vec{p}_4)$, $p_5 = (\omega_5, \vec{p}_5)$ are the momenta of the photon, incident proton, outgoing proton and π^-, π^+ outgoing pions respectively. In (2) ϕ_{45}, θ_{45} are the azimutal and polar angles of $\vec{p}_4$ with respect to $\vec{p}_5$ and θ_5 is the angle of $\vec{p}_5$ with the z direction defined by the incident photon momentum $\vec{k}$. T is the invariant matrix element for the reaction which is derived from a straight application of the Feynman rules of Appendix B.

In fig.3 we show the results of our model separating the terms involving only deltas or deltas and nucleons in the intermediate states (diagrams 12 to 32 in fig. 2) (we refer to the diagrams in fig. 2 in what follows), $N'^*(1520)$ (diagrams 64, 65, 66), $\rho - meson$ (diagrams 51 to 63), non resonant terms (diagrams 1 to 11) and the rest of the diagrams. The diagrams 64, 65 and 66, although they provide a small contribution by themselves, are very relevant when added to the rest of the terms because of the interference of the diagrams 64 and 65 with diagrams 12 and 13, which are the dominant terms in the reaction. For the rest of the terms, their different structure in terms of the momenta of the initial and final particles, together with the different combinations of momenta of these final states allowed by phase space makes the interference very weak and the cross sections practically sum incoherently.

In fig.3 we observe that the Δ terms are clearly the dominant ones, starting at very low energies, in spite of the fact that these terms vanish at threshold. This reflects the weakness of the non resonant terms. These latter terms provide a small background which grows moderately as a function of the energy. The ρ terms are negligible up to $E_\gamma = 800 - 900\ MeV$, but they become relevant at energies above $E_\gamma = 1100\ MeV$ and show up clearly in invariant

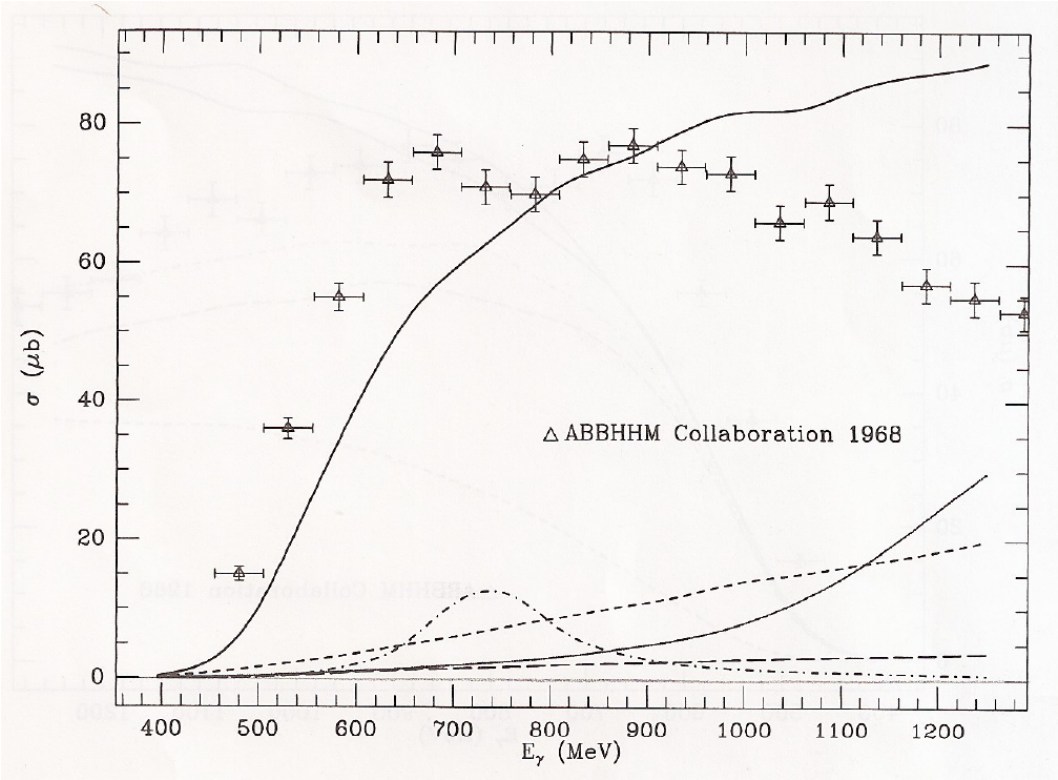

Figure 3: Comparison between different groups of diagrams. Continuous line: Contribution of intermediate Δ states (diagrams 12 to 32 of fig. 2). Dotted line: same from the $\rho - meson$ terms (diagrams 15 to 63). Dot-dashed line: contribution of intermediate $N^*(1520)$ states (diagrams 64, 65 and 66). Short dashed line: contribution of non resonant terms (diagrams 1 to 11). Long dashed line: rest of diagrams.

mass spectra as we shall see later. The terms of the fourth block which involve N^* intermediate states provide a very small contribution, attributable to the weak couplings of the N^* to photons, nucleons and deltas. The N'^* terms which we consider peak around $E_\gamma \simeq 750\ MeV$ and by themselves are even more important than the other non delta terms. Furthermore, when they are added coherently to the delta terms their effect becomes much more relevant as we shall see later on.

By comparison to the $\pi N \longrightarrow \pi\pi N$ reaction [10], some different features are worth mentioning. In the $\pi N \longrightarrow \pi\pi N$ reaction the role of the nonresonant terms is more important than here and dominate the cross section at energies close to threshold. On the other hand, the role of the Δ terms in the $\pi N \longrightarrow \pi\pi N$ reaction is far less relevant than here. What makes the Δ terms particularly important here is the presence of the gauge Kroll Ruderman terms (diagrams 12 and 13). The structure of these diagrams is such that the pion from the $\Delta N\pi\gamma$ vertex can take the right amount of energy to leave the Δ on shell and this coupling, $\vec{S}^\dagger \cdot \vec{\varepsilon}$ is independent of the pion momentum. Because of the structure of this latter vertex these terms have only one derivative coupling and are proportional to one pion momentum. By contrary the Δ terms in the $\pi N \longrightarrow \pi\pi N$ reaction were proportional to two pion momenta, which made them very small close to pion threshold. In the case of the $\pi N \longrightarrow \pi\pi N$ reaction the N^* terms were relevant, while here they provide a very small contribution. What made the N^* contribution particularly relevant in the $\pi N \longrightarrow 2\pi N$ reaction were the terms analogous to diagrams 33 and 34 substituting the photon by the incoming pion. These terms gave an important contribution close to threshold. Here the small $N^*N\gamma$ coupling, together with

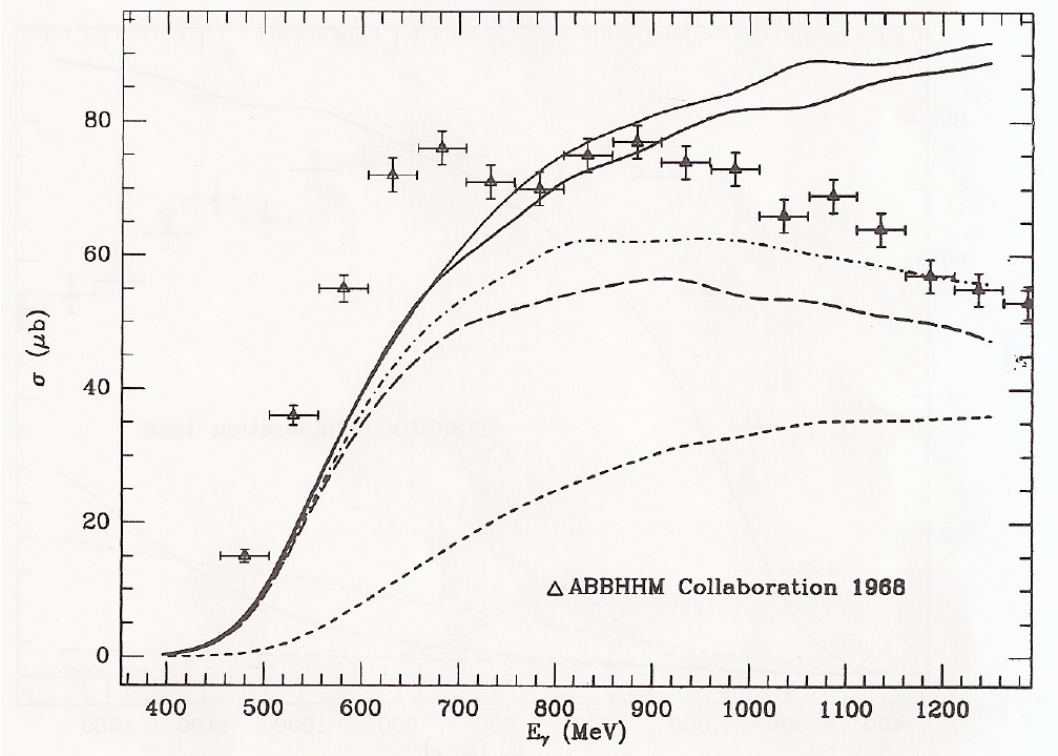

Figure 4: Analysis of the Δ contribution. Continuous line: all terms containing Δ intermediate states (diagrams 12 to 32). Dotted line: dominant terms (diagrams 12, 13, 16, 17, 24, 25 and 32). Long dashed line: Kroll Ruderman Term (diagrams 12, 13) short dashed line: Pion pole term (diagrams 16, 17) Dashed-dotted line: Kroll Ruderman and pion pole terms together (diagrams 12, 13, 16, 17).

the relevance of the Kroll Ruderman term even at small energies, make these N^* terms relatively less important than in the $\pi N \longrightarrow \pi\pi N$ reaction.

Given the relevance of the Δ terms, we show in fig. 4 with more detail the contribution of the different Δ terms. We observe that the Kroll Ruderman (diagrams 12,13) and pion pole (diagrams 16,17) terms dominate the reaction at all energies in the figure, but above $E_\gamma = 700\ MeV$ the contribution of the rest of the Δ terms (essentially diagrams 24, 25, 32) becomes more relevant.

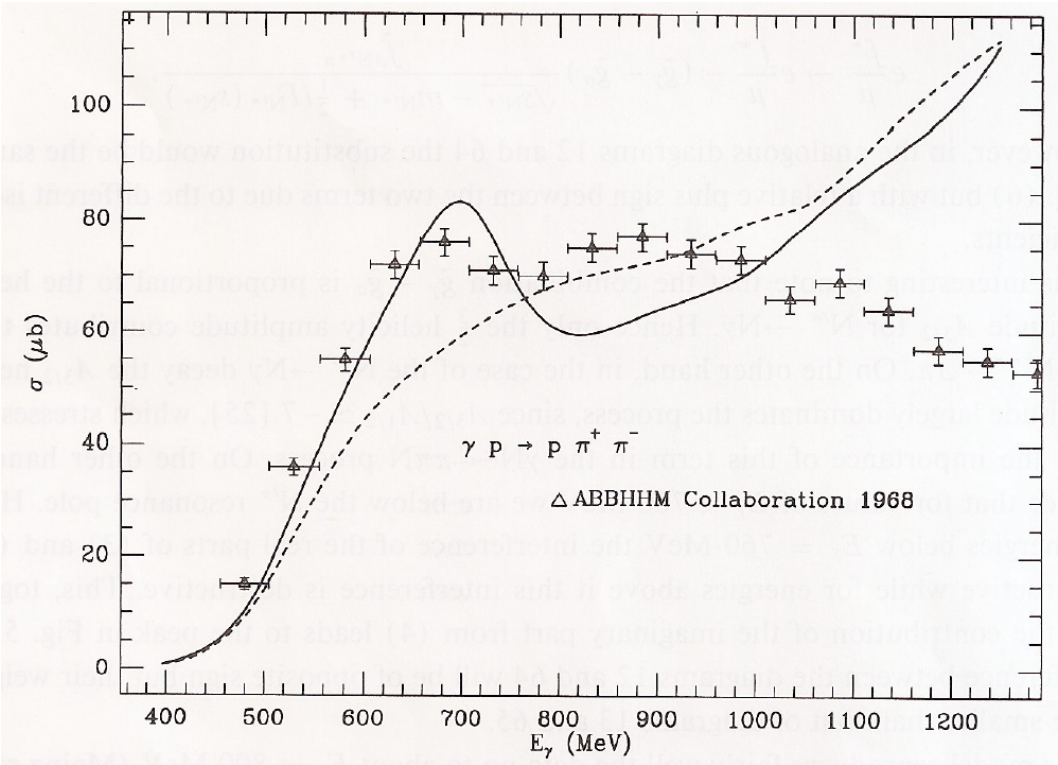

Figure 5: Total cross section. Dashed line: the whole model omitting the $N^*(1520)$ terms of diagrams 64, 65 and 66. Continuous line: complete model.

These Δ diagrams are those considered in ref. [4]. However, we can see that these terms alone fail to reproduce the experimental data.

The ρ contribution is only relevant at high energies as we have already seen. Practically all the contribution from these terms comes from diagrams 51, 52, 56, 57 and among these, the diagrams 51 and 52 provide the dominant contribution.

In fig.5 we show the total cross section including and omitting the $N^*(1520)$ terms of diagrams 64, 65, 66. We can see that with the omission of the $N^*(1520)$ terms the qualitative features of the cross section are not very well reproduced. Our cross section raises monotonically without any peak structure which appears clearly in the experiment. It is worth realizing that in spite of

having delta dominance in the process, the Δ appears on the final πN states and hence the Δ peak does not show up in the cross section as a function of the photon energy. On the other hand, the inclusion of the $N^*(1520)$ terms leads to an interference with the Kroll Ruderman terms which is responsible for the appearance of the maximum and a much better agreement with experiment. This interesting finding shows that although intuitive, it is not correct to associate the peak of the cross section to the Δ resonance. We showed that the delta terms do not lead to such a peak and it comes as an interference phenomenon.

In order to show how this interference appears we write below the amplitudes for the diagrams 13 and 65:

$$-iT_{13} = \frac{f^*}{\mu}\vec{S}\cdot\vec{q}_+\frac{i}{\sqrt{s_\Delta}-m_\Delta+\frac{i}{2}\Gamma_\Delta(s_\Delta)}\,e\,\frac{f^*}{\mu}\,\vec{S}^\dagger\cdot\vec{\varepsilon} \tag{3}$$

$$-iT_{65} = \frac{f^*}{\mu}\vec{S}\cdot\vec{q}_+\frac{i}{\sqrt{s_\Delta}-m_\Delta+\frac{i}{2}\Gamma_\Delta(s_\Delta)}\tilde{f}_{\Delta N'^*\pi}\frac{1}{\sqrt{s_{N'^*}}-m_{N'^*}+\frac{i}{2}\Gamma_{N'^*}(s_{N'^*})}$$
$$\left[-\tilde{g}_\gamma\vec{S}^\dagger\cdot\vec{\varepsilon}+i\tilde{g}_\sigma\left(\vec{S}^\dagger\times\vec{\sigma}\right)\cdot\vec{\varepsilon}\right] \tag{4}$$

Now one can prove that

$$iS_i\left(\vec{S}^\dagger\times\vec{\sigma}\right)\cdot\vec{\varepsilon}=S_i\,\vec{S}^\dagger\cdot\vec{\varepsilon} \tag{5}$$

and as consequence T_{65} has the same structure as T_{13} and the sum of the two can be cast as eq. (3) substituting

$$e\frac{f^*}{\mu}\longrightarrow e\frac{f^*}{\mu}-(\tilde{g}_\gamma-\tilde{g}_\sigma)\frac{\tilde{f}_{\Delta N'^*\pi}}{\sqrt{S_{N'^*}}-m_{N'^*}+\frac{i}{2}\Gamma_{N'^*}(S_{N'^*})} \tag{6}$$

However in the analogous diagrams 12 and 64 the substitution would be the same as in eq. (6) but with a relative + sign between the two terms due to the different isospin coefficients.

It is interesting to note that the combination $\tilde{g}_\gamma - \tilde{g}_\sigma$ is proportional to the helicity amplitude $A_{3/2}$ for $N'^* \longrightarrow N\gamma$. Hence only the 3/2 helicity amplitude contributes to the $\gamma N \longrightarrow N'^* \longrightarrow \Delta\pi$. On the other hand, in the case of the $N'^* \longrightarrow N\gamma$ decay the $A_{3/2}$ helicity amplitude largely dominates the process, since $A_{3/2}/A_{1/2} \simeq -7$ [25], which stresses once more the importance of this term in the $\gamma N \longrightarrow \pi\pi N$ process. On the other hand we can see that for values of $E\gamma < 760\ MeV$ we are below the N'^* resonance pole. Hence, for energies below $E_\gamma = 760\ MeV$ the interference of the real parts of (3) and (4) is constructive while for energies above it this interference is destructive. This, together with the contribution of the imaginary part from (4) leads to the peak in fig. 5. The interference between the diagrams 12 and 64 will be of opposite sign but their weight is much smaller than that of diagrams 13 and 65.

Our model reproduces fairly well the data up to about $E_\gamma = 800\ MeV$ (Mainz range) and from there on the discrepancies are about 20% up to about $E_\gamma = 1100\ MeV$. The fall down of the cross section from $E_\gamma = 900\ MeV$ up is not reproduced by our model which provides a steady increase of the cross section. With $\sqrt{s} = 1520\ MeV$ at $E_\gamma = 760\ MeV$ we should note that many more resonances than those considered by us would play a role from this energy on. Hence there is no reason why our model should work at these energies and we should expect larger discrepancies of our results with the data as the energy increases, which is indeed the case. Even so, within our own model we have neglected terms containing two N^* and those involving the $\Delta N^*\gamma$ vertex. Either because the N^* couplings are small, or because one resonance appears before the γ is absorbed, or both, these diagrams are expected to be small in

the region below $E_\gamma = 800\ MeV$. We have also neglected terms involving N^* intermediate states and ρ coupling given the smallness of the equivalent terms with Δ intermediate states and the smaller couplings of the N^*.

Another limitation of our model where improvements could be done, is in the lack of unitarity. Unitarity of the amplitude with three particles in the final state is a rather difficult problem [32]. In what concerns unitarity in the πN channel, our model is near unitary, given the dominance of the delta terms and the fact that the Δ width is implemented in the Δ propagators. We have made some estimates on the order of magnitude of the corrections that implementing unitarity could bring. For this purpose we follow the procedure of Olson [33] to unitarize this channel by multiplying the Δ terms by a phase and requesting that the resulting amplitude, after adding the background, has the phase of the πN amplitude. The angle φ of the phase $e^{i\varphi}$ is of the order of 10°. We have checked that implementing this phase in the amplitude changes the results at the level of 3 %. Even increasing the angle φ to 20° the changes are of the same order of magnitude. Crude as this estimate is for such an involved problem, however, it gives hints that the corrections might be small. Nevertheless, a serious treatment of this problem would be welcome.

3.2 Invariant mass distribution

It is also instructive to look at distributions of invariant masses. The formulas for $d\sigma/dM_I$ are easily obtained by multiplying eq. (1) by

$$\int dM_I^2\, \delta(M_I^2 - (p_i + p_j)^2) \tag{7}$$

with p_i, p_j the momenta of the pair of particles which we consider.

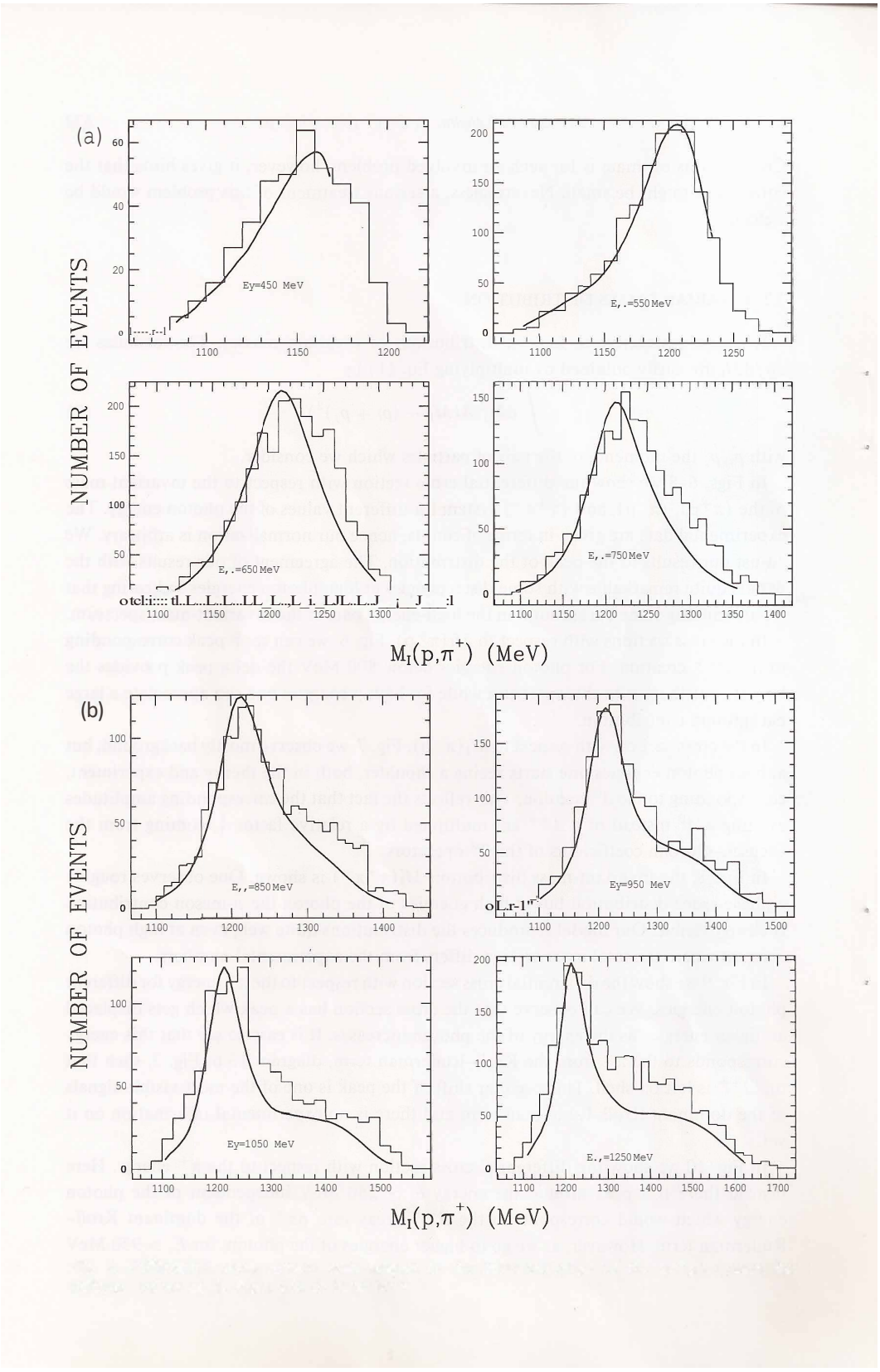

Figure 6: Differential cross section with respect to the invariant mass of the $(\pi^+ p)$ system for different values of E_γ^{lab} from 450 MeV to 1250 MeV.

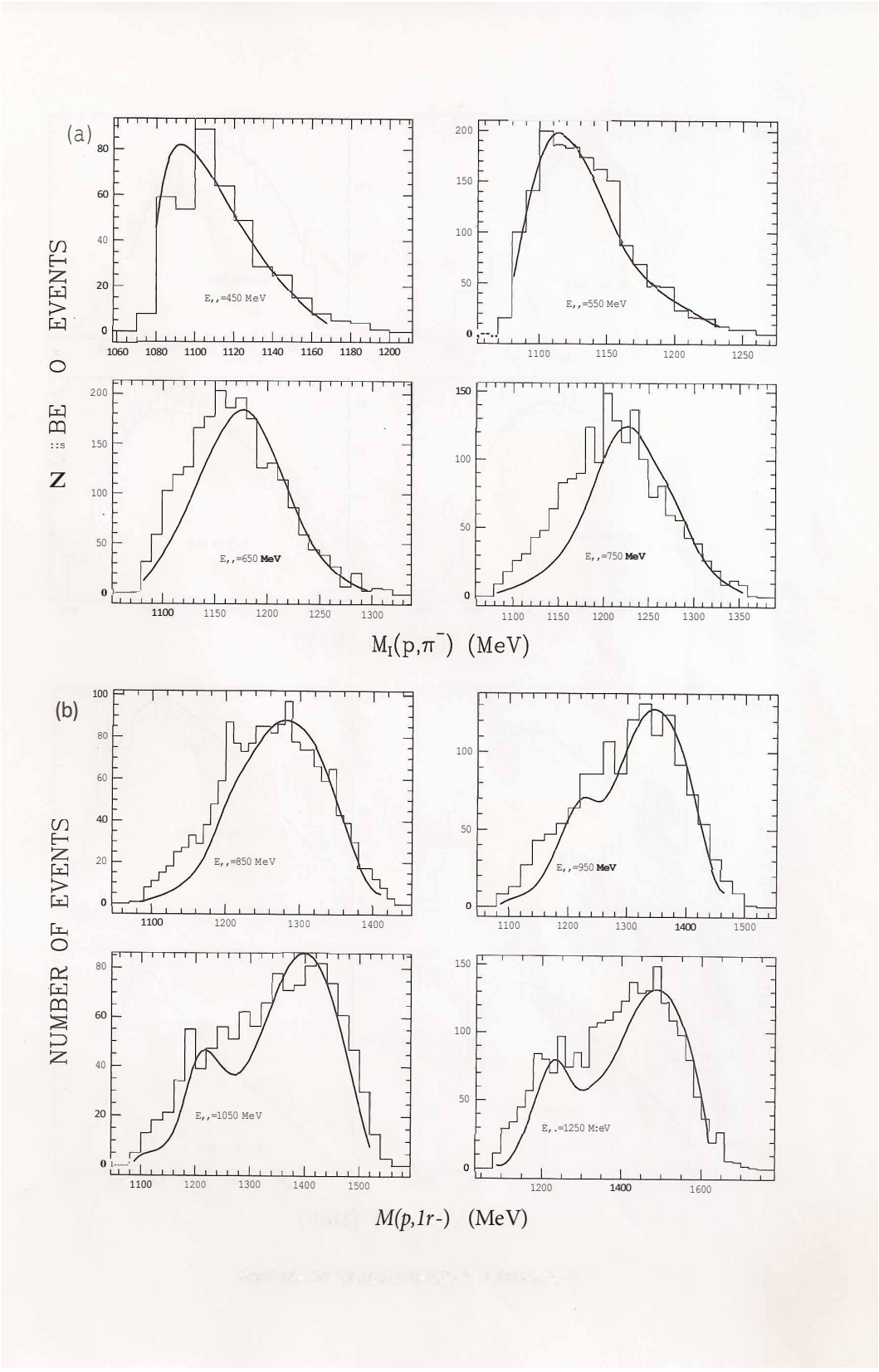

Figure 7: Same as fig. 6 for the $(\pi^- p)$ system.

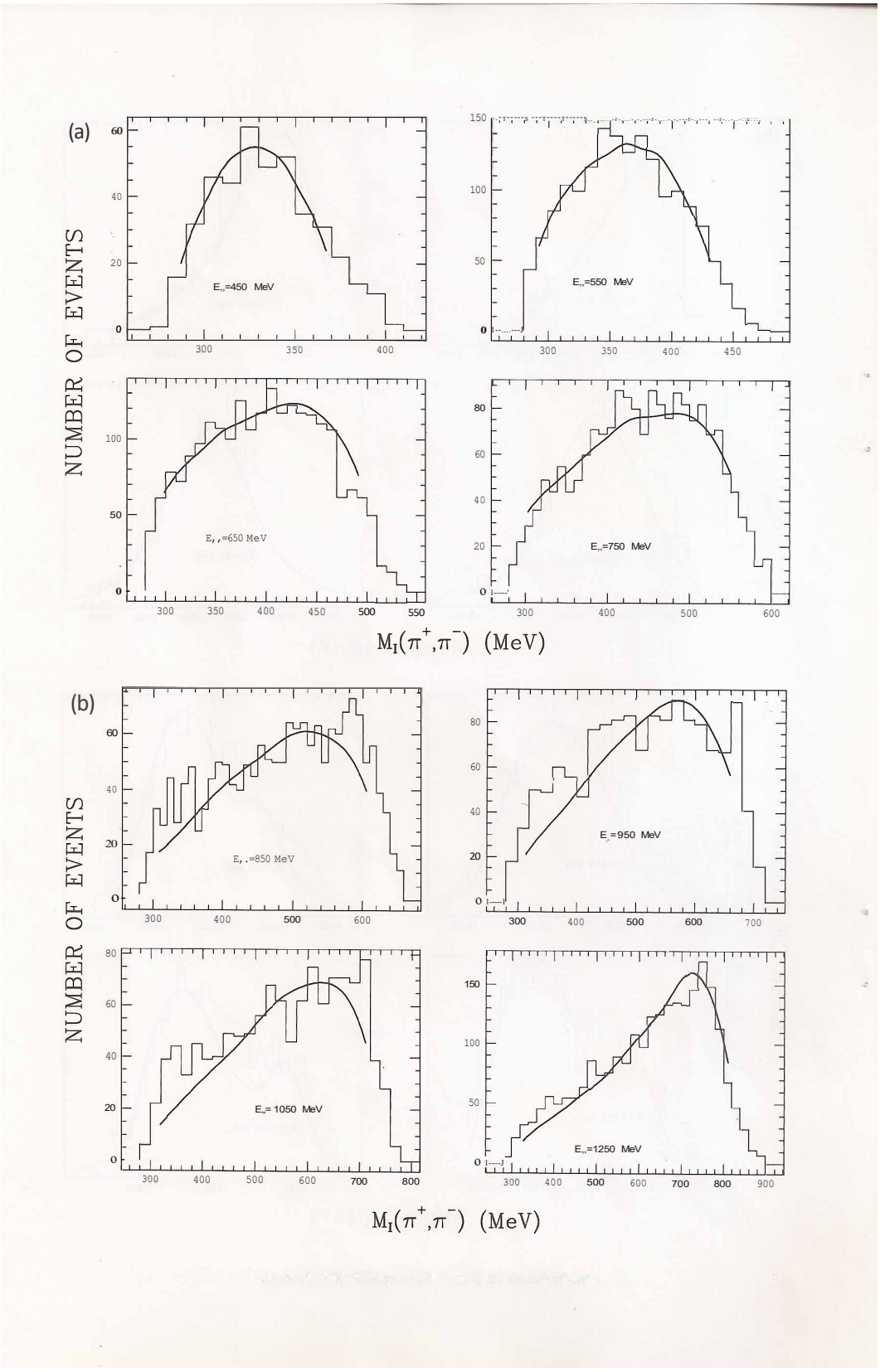

Figure 8: Same as fig. 6 for the $(\pi^+\pi^-)$ system.

In figs. 6-8 we show the differential cross section with respect to the invariant mass of the $(\pi^+ p)$, $(\pi^- p)$, and $(\pi^+\pi^-)$ system for different values of the photon energy. The experimental data are given in terms of counts, hence our normalization is arbitrary. We adjust our results to the peak of the distribution. The agreement of our results with the data is quite remarkable with some discrepancies at high photon energies indicating that we are missing some background in the high energy part of the invariant mass spectrum.

In the cross sections with respect to $M_I(\pi^+ p)$, fig. 6, we can see a peak corresponding to the Δ^{++} creation. For photon energies below 800 MeV the delta peak provides the largest contribution to this spectrum while for high γ energies one can appreciate a large background contribution.

In the cross section with respect to $M_I(\pi^- p)$, fig. 7, we observe mostly background, but at high photon energies one starts seeing a shoulder, both in the theory and experiment, corresponding to the Δ^o creation. This reflects the fact that the corresponding amplitudes exciting a Δ^o instead of a Δ^{++} are multiplied by a relative factor 1/3, coming from the Clebsch Gordan coefficients of the T^λ operators.

In fig. 8, the invariant mass distribution $M_I(\pi^+\pi^-)$ is shown. One observes roughly a phase space distribution but at high energies of the photon the ρ meson contribution is clearly visible. Our model reproduces the distributions quite well, even at high photon energies where the total cross section differs from the experimental numbers.

In fig. 9 we show the differential cross section with respect to the π^- energy for different photon energies. We can observe that the cross section has a peak which gets displaced at higher energies as the energy of the photon increases. It

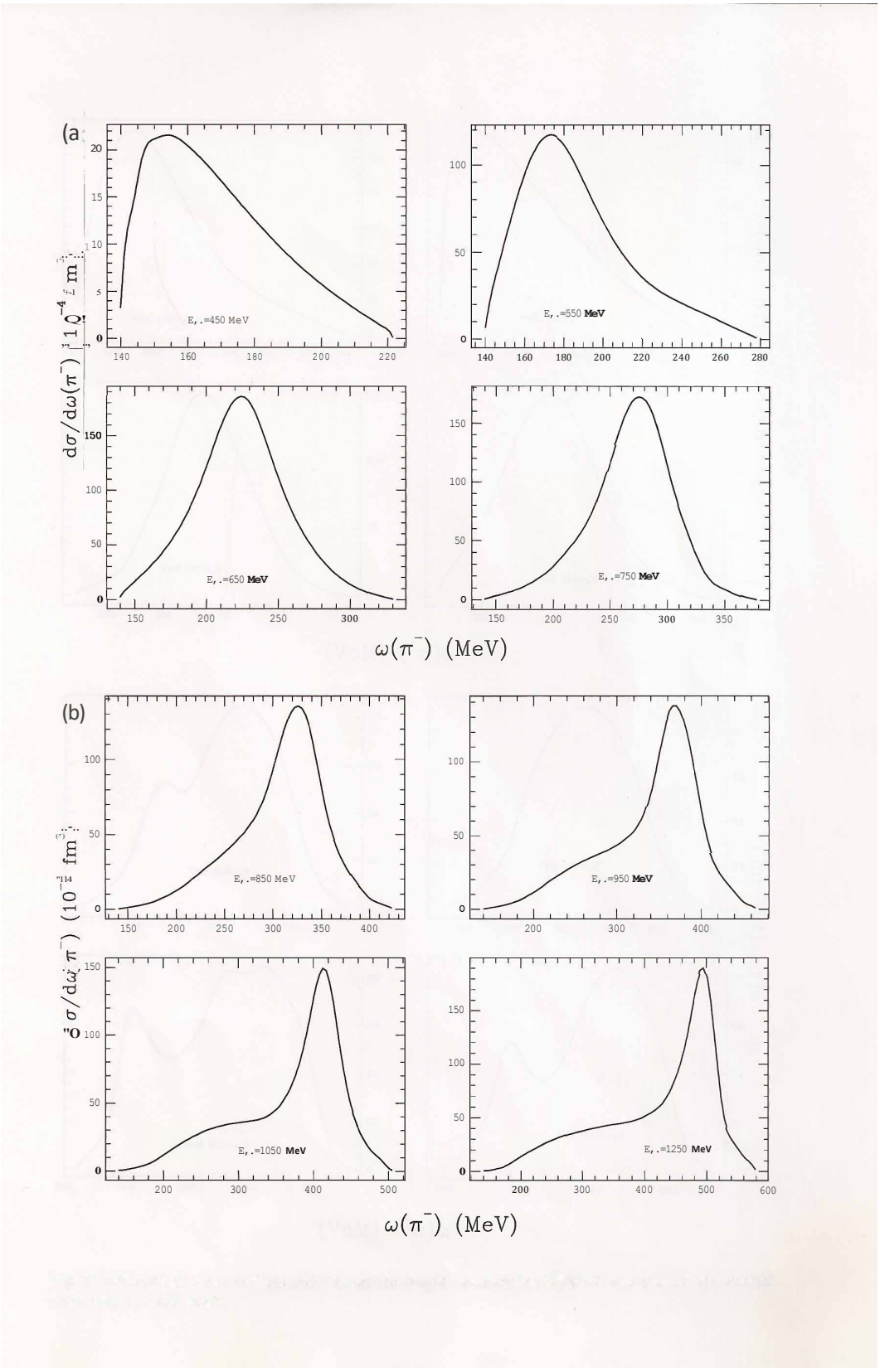

Figure 9: Differential cross section with respect to the π^- energy for different energies of the photon between 450 MeV to 1250 MeV.

is easy to see that this energy corresponds to the π^- from the Kroll Ruderman term, diagram 13 of fig. 2, such that the Δ^{++} is left on shell. This peculiar shift of the peak is one of the most visible signals of the dominant Kroll Ruderman term and there is no experimental information on it yet.

In fig. 10 we show he differential cross section with respect to the π^+ energy. Here instead there is a peak around the energy $\omega \simeq 250\ MeV$ independent of the photon energy which would correspond to the Δ^{++} decay into $p\pi^+$ of the dominant Kroll Ruderman term. However, as we go to higher energies of the photon, for $E_\gamma > 950\ MeV$ we observe a second peak in the same position as in fig. 9, which could be interpreted as the contribution from the Kroll Ruderman term of diagram 12 of fig. 2 when a Δ^o is formed and a π^+ emitted from the $\Delta N\pi\gamma$ vertex. As commented above, the strength of this diagram is 1/3 of the diagram 13. The peak corresponding to the one seen in fig. 9 would be present here but with much smaller strength. Hence, if this peak falls in the region of the Δ decay peak of fig. 10 it will not show up, but if it occurs at the tail of the Δ decay distribution, as it happens at photon energies above 950 MeV, that peak has more chances to be visible as it is the case.

The detailed study of invariant mass and energy distributions clearly shows many of the dynamical features of the mechanisms responsible for the reaction.

4 Conclusions:

We have constructed a model for the $\gamma p \longrightarrow \pi^+\pi^- p$ reaction including nucleons, $\Delta(1232)$, $N^*(1440)$ and $N^*(1520)$ as intermediate baryonic states as well as $\rho - meson$ intermediate states for the $\pi^+\pi^-$ system. Our model accounting

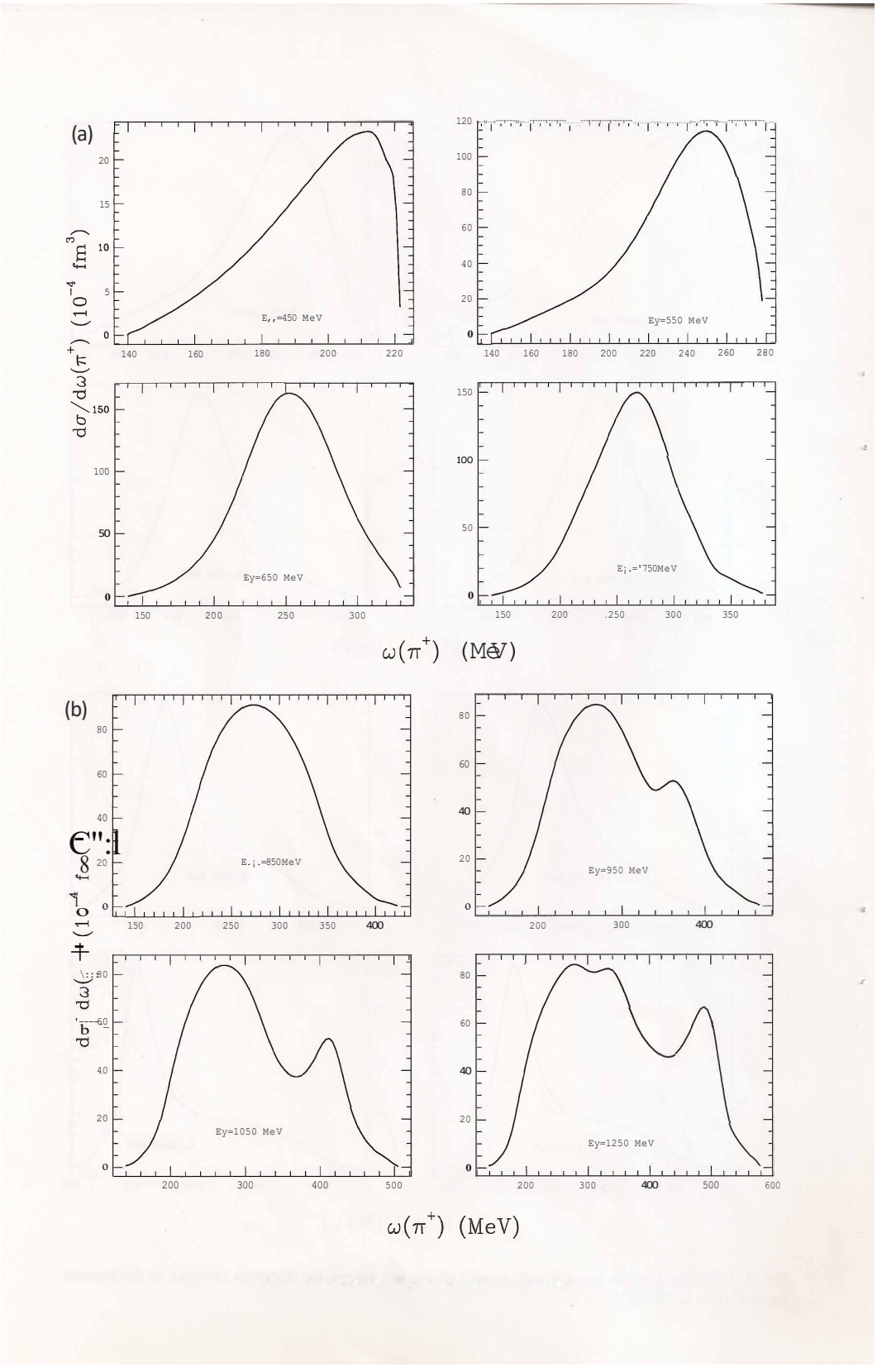

Figure 10: Same as fig. 9 for the π^+.

for 67 Feynman diagrams is rather complete, but still misses terms which become relevant from $E_\gamma = 800\ MeV$ on. As in a previous model accounting for only a few of these diagrams we observe the dominance of the Kroll Ruderman and pion pole terms but get an appreciable contribution from other terms. In particular we found the contribution of the $N^*(1520)$ resonance very important, and essential to produce the peak which is present in the experimental cross section around $E_\gamma = 680\ MeV$. With respect to the $\pi N \longrightarrow 2\pi N$ reaction the present one presents novelties. First it is dominated by Δ terms even at low energies close to threshold and non resonant terms have little strength in the reaction. This is in contrast to the $(\pi, 2\pi)$ reaction where the background non resonant terms were very important at low energies and the Δ terms is general rather small. Another feature which differences both reactions is the role of the N^* intermediate states which was important at low energies in the $\pi N \longrightarrow \pi\pi N$ reaction and is negligible in $\gamma p \longrightarrow \pi^+\pi^- p$.

We have also studied differential cross sections with respect to the energy of the π^+ and π^- and have observed features which are very much tied to dynamical aspects of the reaction mechanisms assumed. Such experimental information is not available and the reopening of the investigation of this reaction at Mainz with the large acceptance detector DAPHNE or with the photon spectrometer TAPS makes advisable this kind of measurement as useful tools to pin down the dynamics of the process.

Most of the information used has a phenomenological origin and is tied to decay widths of resonances into partial channels. In unknown cases we have used the quark model as a way to obtain coupling constants, in other cases we use it to provide the sign and get the strength from some partial decay rate.

One piece of information we introduced using the experimental data. This was the $N^*(1520)\Delta\pi$ vertex. The simplest vertex structure compatible with all the symmetries is assumed but the sign of the term is fixed by the requirement of better fitting the data. There was no doubt in the choice since the two signs gave rise to two different cross sections, one of them clearly incompatible, even qualitatively, with experiment. In this sense what we are saying is that this reaction has the information to provide some interesting couplings, with sign included, which can not be obtained from the study of other reactions so far analysed. It would also be interesting to perform some quark model calculation for this decay which is technically more elaborate than the evaluation of N and Δ matrix elements where ratios of couplings can be easily obtained without detailed calculations since the radial matrix elements are the same in both cases.

On the other hand studies already done and other preliminary results indicate that the present reaction in nuclei has interesting renormalization effects. The model developed here is sufficiently realistic and accurate below $E_\gamma = 800$ MeV to be used for the study of the $(\gamma, 2\pi)$ reaction in nuclei, which should become a natural continuation of the elementary $(\gamma, 2\pi)$ reaction.

Acknowledgements: We are indebted to S.M. Singh who provided us with relevant information on the $N^*N\gamma$ coupling. Discussions with J. Bernabeu, F. Botella, P. González, S. Noguera, J. Peñarrocha and M.J. Vicente-Vacas are warmly acknowledged. This work has been partially supported by CICYT contract number AEN 90-049. One of us J.A. Gómez-Tejedor wishes to acknowledge financial support from the Institució Valenciana d'Estudis i Investigació.

Appendix A

LAGRANGIANS.

$$\mathcal{L}_{NN\pi} = \frac{-f}{\mu}\,\overline{\Psi}\gamma^{\mu}\gamma_5\partial_{\mu}\vec{\phi}\vec{\tau}\,\Psi \tag{A.1}$$

$$\mathcal{L}_{NN\pi\pi} = -4\pi\frac{\lambda_1}{\mu}\,\overline{\Psi}\vec{\phi}\vec{\phi}\Psi \tag{A.2}$$

$$\mathcal{L}_{\Delta N\pi} = \frac{-f^*}{\mu}\Psi^{\dagger}_{\Delta}S_i(\partial_i\phi^{\lambda})T^{\lambda}\Psi_N \;+\; h.c. \tag{A.3}$$

$$\mathcal{L}_{\Delta\Delta\pi} = \frac{-f_{\Delta}}{\mu}\Psi^{\dagger}_{\Delta}S_{\Delta i}(\partial_i\phi^{\lambda})T^{\lambda}_{\Delta}\Psi_{\Delta} \;+\; h.c. \tag{A.4}$$

$$\mathcal{L}_{NN^*\pi} = \frac{-\tilde{f}}{\mu}\Psi^{\dagger}_{N^*}\sigma_i\left(\partial_i\vec{\phi}\right)\vec{\tau}\,\Psi_N \;+\; h.c. \tag{A.5}$$

$$\mathcal{L}_{NN^*\pi\pi} = -C\overline{\Psi}_{N^*}\vec{\phi}\vec{\phi}\,\Psi_N \;+\; h.c. \tag{A.6}$$

$$\mathcal{L}_{\Delta N^*\pi} = \frac{-g_{\Delta N^*\pi}}{\mu}\Psi^{\dagger}_{\Delta}S_i(\partial_i\phi^{\lambda})T^{\lambda}\Psi_{N^*} \;+\; h.c. \tag{A.7}$$

$$\mathcal{L}_{\Delta N'^*\pi} = i\tilde{f}_{\Delta N'^*\pi}\overline{\Psi}_{N'^*}\phi^{\lambda}T^{\lambda}\Psi_{\Delta} \;+\; h.c. \tag{A.8}$$

$$\mathcal{L}_{NN\gamma} = -e\overline{\Psi}_N(\gamma^\mu A_\mu - \frac{\chi_N}{2m}\sigma^{\mu\nu}\partial_\nu A_\mu)\Psi_N \tag{A.9}$$

$$\mathcal{L}_{\pi\pi\gamma} = ie(\phi_+\partial^\mu\phi_- \ - \ \phi_-\partial^\mu\phi_+)A_\mu \tag{A.10}$$

$$\mathcal{L}_{NN\pi\gamma} = -i\mathsf{q}\frac{f}{\mu}\,\overline{\Psi}\gamma^\mu\gamma_5 A_\mu\vec{\phi}\vec{\tau}\,\Psi \tag{A.11}$$

$$\mathcal{L}_{\Delta N\pi\gamma} = -i\mathsf{q}\frac{f^*}{\mu}\Psi^\dagger_\Delta S_i A_i\phi^\lambda T^\lambda\Psi_N \ + \ h.c. \tag{A.12}$$

$$\mathcal{L}_{NN^*\pi\gamma} = -i\mathsf{q}\frac{\tilde{f}}{\mu}\mathsf{q}\Psi^\dagger_{N^*}\sigma_i A_i\vec{\phi}\vec{\tau}\,\Psi_N \ + \ h.c. \tag{A.13}$$

$$\mathcal{L}_{\Delta N\gamma} = \frac{-f_{\Delta N\gamma}}{\mu}\Psi^\dagger_\Delta\epsilon_{ijk}S^\dagger_i\left(\partial_j A_k\right)T_3\Psi_N \ + \ h.c. \tag{A.14}$$

$$\mathcal{L}_{N^*N\gamma} = \frac{\tilde{f}^N_\gamma}{\mu}\,\overline{\Psi}_N\sigma^{\mu\nu}\partial_\nu A_\mu\Psi_{N^*} \ + \ h.c. \tag{A.15}$$

$$\mathcal{L}_{N'^*N\gamma} = \overline{\Psi}_N\left\{\tilde{g}_\gamma\vec{S}\vec{A} \ - \ i\tilde{g}_\sigma\left(\vec{\sigma}\times\vec{S}\right)\vec{A}\right\}\Psi_{N'^*} \ + \ h.c. \tag{A.16}$$

$$\mathcal{L}_{NN\rho} = -\overline{\Psi}\left\{G^V_{NN\rho}\,\gamma^\mu\vec{\phi}^{(\rho)}_\mu \ - \ \frac{G^T_{NN\rho}}{2m}\,\sigma^{\mu\nu}\partial_\nu\vec{\phi}^{(\rho)}_\mu\right\}\vec{\tau}\Psi \tag{A.17}$$

$$\mathcal{L}_{\rho\pi\pi} = -f_\rho \, \vec{\phi}_\mu^{(\rho)} \left(\vec{\phi} \times \partial^\mu \vec{\phi} \right) \tag{A.18}$$

$$\mathcal{L}_{N\Delta\rho} = -\sqrt{C_\rho} \, \frac{f^*}{\mu} \Psi_\Delta^\dagger \epsilon_{ijk} S_i \left(\partial_j \phi_k^{(\rho)\lambda} \right) T^\lambda \Psi \; + \; h.c. \tag{A.19}$$

$$\mathcal{L}_{N'^* N \rho^0} = -\tilde{g}_\rho \overline{\Psi}_N S_i \phi_i^{(\rho)} \Psi_{N'^*} \; + \; h.c. \tag{A.20}$$

$$\mathcal{L}_{\rho\pi\gamma} = \frac{g_{\rho\pi\gamma}}{\mu} \epsilon^{\alpha\beta\gamma\delta} \, \partial_\alpha A_\beta \vec{\phi} \, \partial_\gamma \vec{\phi}_\delta^{(\rho)} \tag{A.21}$$

$$\mathcal{L}_{\rho^0\pi^+\pi^-\gamma} = e f_\rho \phi_\mu^{(\rho)} \left(\phi_+ A^\mu \phi_- \; + \; \phi_- A^\mu \phi_+ \right) \tag{A.22}$$

$$\mathcal{L}_{\pi\pi\pi\gamma} = \frac{F^{3\pi}}{6} \epsilon^{\mu\nu\alpha\beta} \epsilon^{abc} \, A_\mu \, \partial_\nu \phi^a \, \partial_\alpha \phi^b \, \partial_\beta \phi^c \tag{A.23}$$

$$\mathcal{L}_{\pi\gamma\gamma} = \frac{F^\pi}{4} \epsilon^{\mu\nu\alpha\beta} \phi^0 F_{\mu\nu} F_{\alpha\beta} \tag{A.24}$$

$$F_{\mu\nu} = \partial_\mu A_\nu \; - \; \partial_\nu A_\mu$$

In these expressions, Ψ, $\vec{\phi}$, Ψ_Δ, Ψ_{N^*}, $\Psi_{N'^*}$, $\vec{\phi}_\mu^{(\rho)}$ and A_μ stand for the nucleon, pion, $\Delta(1232)$, $N^*(1440)$, $N^*(1550)$, $\rho(770)$ and photon fields, respectively; m and μ are the nucleon and pion masses. The coupling constants are listed below.

Coupling constants:

$\frac{f^2}{4\pi} = 0.08$ $\lambda_1 = 0.0075$

$\frac{f^{*2}}{4\pi} = 0.36$ $f_\Delta = 0.802$

$\tilde{f} = 0.472$ $C = -2.66\mu^{-1}$

$g_{\Delta N^*\pi} = 1.784$ $\tilde{f}_{\Delta N'^*\pi} = 0.677$

$e = 0.30282$ $\chi_N = \begin{cases} 1.79 & for\ proton \\ -1.91 & for\ neutron \end{cases}$

$f_{\Delta N\gamma} = 0.116$ $\tilde{f}^N_\gamma = \begin{cases} 0.0147 & for\ proton \\ -0.0084 & for\ neutron \end{cases}$

$\tilde{g}_\gamma = 0.108$ $\tilde{g}_\sigma = -0.049$

$G^V_{NN\rho} = 2.9$ $G^T_{NN\rho} = 18.15$

$f_\rho = 6.14$ $C_\rho = 2$

$\tilde{g}_\rho = 0.591$ $g_{\rho\pi\gamma} = 0.03774$

$F^{3\pi} = 0.0259\mu^{-3}$ $F^\pi = 0.0035\mu^{-1}$

Appendix B

Feynman rules corresponding to the diagrams in fig. 11.

$$-i\delta H_{NN\pi} = \frac{-f}{\mu}\left(\vec{\sigma}\cdot\vec{q} - q^0\frac{\vec{\sigma}\cdot(\vec{p}+\vec{p}')}{2m}\right)\tau^\lambda \tag{B.1}$$

$$-i\delta H_{NN\pi\pi} = \frac{-i8\pi\lambda_1}{\mu} \tag{B.2}$$

$$-i\delta H_{\Delta N\pi} = \frac{-f^*}{\mu}\vec{S}\cdot\vec{q}\,T^\lambda \tag{B.3}$$

$$-i\delta H_{\Delta\Delta\pi} = \frac{-f_\Delta}{\mu}\vec{S}_\Delta\cdot\vec{q}\,T^\lambda_\Delta \tag{B.4}$$

$$-i\delta H_{NN^*\pi} = \frac{-\tilde{f}}{\mu}\,\vec{\sigma}\cdot\vec{q}\,\tau^\lambda \tag{B.5}$$

$$-i\delta H_{NN^*\pi\pi} = -i\,2\,C \tag{B.6}$$

$$-i\delta H_{\Delta N^*\pi} = \frac{-g_{\Delta N^*\pi}}{\mu}\vec{S}\cdot\vec{q}\,T^\lambda \tag{B.7}$$

$$-i\delta H_{\Delta N'^*\pi} = -\tilde{f}_{\Delta N'^*\pi}T^\lambda \tag{B.8}$$

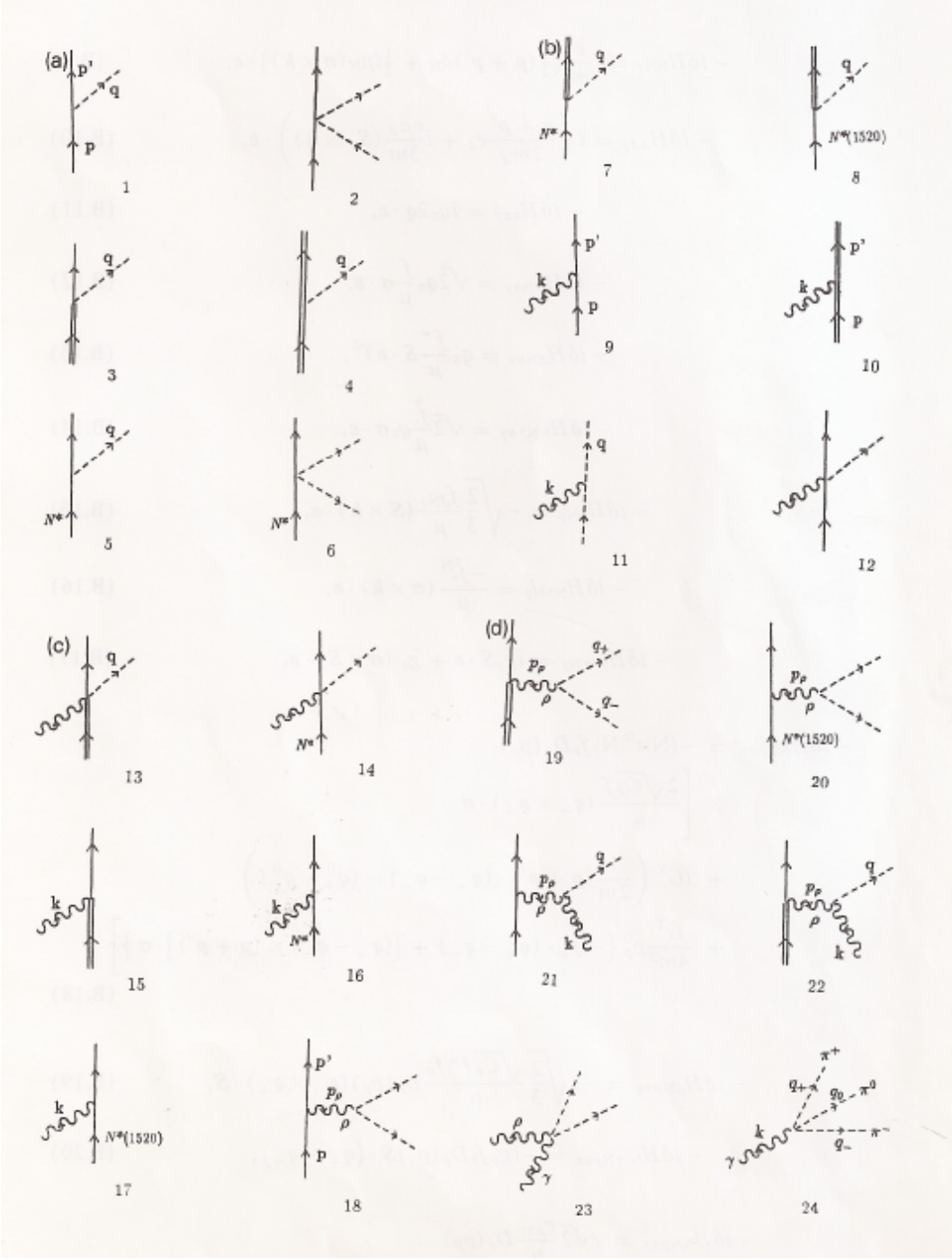

Figure 11: Diagrams for the Feynman rules.

$$-i\delta H_{NN\gamma} = i\frac{e}{m}\left\{\frac{1}{2}(\vec{p}+\vec{p}\,')\delta_N + i\,\frac{\mu_N}{2}(\vec{\sigma}\times\vec{k}\,)\right\}\cdot\vec{\varepsilon} \tag{B.9}$$

$$-i\delta H_{\Delta\Delta\gamma} = i\left\{\frac{(\vec{p}+\vec{p}\,')}{2m_\Delta}e_\Delta + i\,\frac{e\mu_\Delta}{3m}(\vec{S}_\Delta\times\vec{k}\,)\right\}\cdot\vec{\varepsilon} \tag{B.10}$$

$$-i\delta H_{\pi\pi\gamma} = i\,\mathsf{q}_\pi\,2\,\vec{q}\cdot\vec{\varepsilon} \tag{B.11}$$

$$-i\delta H_{NN\pi\gamma} = \sqrt{2}\,\mathsf{q}_\pi\frac{f}{\mu}\vec{\sigma}\cdot\vec{\varepsilon} \tag{B.12}$$

$$-i\delta H_{\Delta N\pi\gamma} = \mathsf{q}_\pi\frac{f^*}{\mu}\vec{S}\cdot\vec{\varepsilon}\,T^\lambda \tag{B.13}$$

$$-i\delta H_{NN^*\pi\gamma} = \sqrt{2}\frac{\tilde{f}}{\mu}\,\mathsf{q}_\pi\,\vec{\sigma}\cdot\ \vec{\varepsilon} \tag{B.14}$$

$$-i\delta H_{\Delta N\gamma} = -\sqrt{\frac{2}{3}}\,\frac{f_{\Delta N\gamma}}{\mu}(\vec{S}\times\vec{k}\,)\cdot\vec{\varepsilon} \tag{B.15}$$

$$-i\delta H_{N^*N\gamma} = \frac{-\tilde{f}^N_\gamma}{\mu}(\vec{\sigma}\times\vec{k}\,)\cdot\vec{\varepsilon} \tag{B.16}$$

$$-i\delta H_{N'^*N\gamma} = i\tilde{g}_\gamma\vec{S}\cdot\vec{\varepsilon}\ +\ \tilde{g}_\sigma\left(\vec{\sigma}\times\vec{S}\right)\cdot\vec{\varepsilon} \tag{B.17}$$

$$-i\delta H_{NN\rho\pi\pi} = -\langle N \left|\tau^0\right| N\rangle f_\rho D_\rho(p_\rho) \left\{ \frac{2\sqrt{C_\rho} f}{\mu} (\vec{q}_- \times \vec{q}_+) \cdot \vec{\sigma} + \right.$$

$$iG^V \left[\frac{1}{2m} (\vec{p} + \vec{p}\,') \cdot (\vec{q}_+ - \vec{q}_-) - (q_+^0 - q_-^0) \right] + \tag{B.18}$$

$$\left. \frac{G^T}{4m^2} p_\rho^0 \left[-i\vec{p_\rho} \cdot (\vec{q}_+ - \vec{q}_-) + ((\vec{q}_+ - \vec{q}_-) \times (\vec{p} + \vec{p}\,')) \cdot \vec{\sigma} \right] \right\}$$

$$-i\delta H_{\Delta N\rho\pi\pi} = -2\sqrt{\frac{2}{3}} \frac{\sqrt{C_\rho} f^* f_\rho}{\mu} D_\rho(p_\rho)\ (\vec{q}_- \times \vec{q}_+) \cdot \vec{S} \tag{B.19}$$

$$-i\delta H_{N'^* N\rho\pi\pi} = -ig_\rho f_\rho D_\rho(p_\rho) \vec{S} \cdot (\vec{q}_+ - \vec{q}_-) \tag{B.20}$$

$$-i\delta H_{NN\rho\pi\gamma} = r\sqrt{2}\, \frac{g_{\rho\pi\gamma}}{\mu} D_\rho(p_\rho) \left\{ i \left(G^V + \frac{{p_\rho^0}^2 - {\vec{p}_\rho}^{\,2}}{4m^2} G^T \right) \epsilon_{\alpha i \gamma 0} + \right.$$

$$\left. \frac{1}{2m} (G^V + G^T) \epsilon_{\alpha i \gamma j} (\vec{\sigma} \times \vec{p}_\rho)^j \right\} k^\alpha \varepsilon^i q^\gamma \tag{B.21}$$

$$-i\delta H_{\Delta N\rho\pi\gamma} = r \frac{\sqrt{C_\rho} f^* g_{\rho\pi\gamma}}{\mu^2} D_\rho(p_\rho)\, \epsilon_{\alpha i \gamma j}\ \left(\vec{S} \times \vec{p}_\rho \right)^j\ k^\alpha\, \varepsilon^i\, q^\gamma\, T^\lambda \tag{B.22}$$

$$-i\delta H_{\rho^0\pi^+\pi^-\gamma} = -2ei f_\rho \vec{\varepsilon}^{\,(\rho)} \cdot \vec{\varepsilon} \tag{B.23}$$

$$-i\delta H_{\pi\pi\pi\gamma} = -iF^{3\pi}\, \epsilon_{\mu i \alpha \beta}\, k^\mu\, \varepsilon^i\, q_+^\alpha\, q_-^\beta \tag{B.24}$$

In these expressions $\vec{\tau}$ is the isospin 1/2 operator. $\vec{S}$, $\vec{T}$ are the transition spin and isospin operators from 1/2 to 3/2 with the normalization

$$\langle \frac{3}{2}, M \left| S_\nu^\dagger \right| \frac{1}{2}, m \rangle = C\left(\frac{1}{2}, 1, \frac{3}{2}; m, \nu, M\right) \tag{B.25}$$

with ν in spherical base and same for T.

$\vec{S}_\Delta$, $\vec{T}_\Delta$ appearing in (B.4) and (B.10) are the ordinary spin and isospin matrices for a spin-isospin 3/2, 3/2 object. Some useful relationships employed in the derivation of the amplitudes are

$$\sum_M S_i \left|M\right\rangle\left\langle M\right| S_j^\dagger = \frac{2}{3}\delta_{ij} \; - \; \frac{i}{3}\epsilon_{ijk}\sigma_k \tag{B.26}$$

$$\sum_{MM'} S_i \left|M\right\rangle\left\langle M\right| S_{\Delta j} \left|M'\right\rangle\left\langle M'\right| S_k^\dagger = \frac{5}{6} i\epsilon_{ijk} \; - \; \frac{1}{6}\delta_{ij}\sigma_k \; + \; \frac{2}{3}\delta_{ik}\sigma_j \; - \; \frac{1}{6}\delta_{jk}\sigma_i \tag{B.27}$$

which are found in [10,23].

The value of q_π is the charge ($\pm e$) of the outgoing pion, $\vec{q}$ its momentum and q^0 its energy. $\vec{p}$ y $\vec{p}\,'$ are the momenta of the incident and outgoing nucleons respectively and $\vec{k}$ the photon momentum.

$\vec{\varepsilon}$ is the polarization vector of the photon. We work in the Coulomb gauge ($\varepsilon^0 = 0$, $\vec{\varepsilon}\cdot\vec{k} = 0$); $\vec{\varepsilon}^{(\rho)}$ is the polarization vector of the ρ-meson.

In eq. (B.9) δ_N is 1 for the proton and zero for the neutron, and μ_N is the nucleon magnetic moment.

In eqs. (B.21) and (B.22) r is the pion charge (± 1) in electron charge units.

For the pion fields we use the Bjorken and Drell convention [24]

$$\begin{aligned}
&\phi_+ = \tfrac{1}{\sqrt{2}}\,(\phi_1 - i\phi_2) \quad \textit{destroys } \pi^+,\ \textit{creates } \pi^- \\
&\phi_- = \tfrac{1}{\sqrt{2}}\,(\phi_1 + i\phi_2) \quad \textit{destroys } \pi^-,\ \textit{creates } \pi^+ \\
&\phi_0 = \phi_3 \qquad\qquad\quad \textit{destroys } \pi^0,\ \textit{creates } \pi^0
\end{aligned} \tag{B.28}$$

Hence the $|\pi^+\rangle$ state corresponds to $-\,|1\,1\rangle$ in isospin base. The normalization of the antisymmetric tensor $\epsilon_{\alpha\beta\gamma\delta}$ is also taken from [24] with $\epsilon_{0123} = 1$.

In eq. (B.18) $|N\rangle$ is the nucleon isospin state.

In eq. (B.18) and followings, p_ρ stands for the momentum of the intermediate ρ meson and q_+, q_- for the momenta of the π^+ and π^-.

For the complex conjugate vertices of the figures we obtain contributions to $-i\delta H^\dagger$. Hence the terms such that $-i\delta H$ is real change sign in $-i\delta H^\dagger$ and those which are purely imaginary do not change signs. As an example, the Kroll-Ruderman term $-i\delta H_{\Delta N\pi\gamma}$ (including the phase -1 for the π^+) are all positive when one creates a Δ and all negatives when one destroys a Δ (apart form the spin factor $\vec{S}^{\,\dagger}\cdot\vec{\varepsilon}$ or $\vec{S}\cdot\vec{\varepsilon}$).

For the baryon propagator we take the positive energy part, hence:

$$G_N(p) = \frac{1}{p^0 - E(\vec{p}) + i\varepsilon}\frac{m}{E(\vec{p})} \quad ; \quad E(\vec{p}) = \sqrt{m^2 + \vec{p}^{\,2}} \tag{B.29}$$

$$G_\Delta(p) = \frac{1}{\sqrt{s} - m_\Delta + \frac{i}{2}\Gamma_\Delta(s)}\frac{m_\Delta}{E_\Delta(\vec{p})} \tag{B.30}$$

$$s = {p^0}^2 - \vec{p}^{\,2} \quad ; \quad E_\Delta(\vec{p}) = \sqrt{m_\Delta^2 + \vec{p}^{\,2}}$$

$$\Gamma_\Delta = \frac{2}{3}\frac{1}{4\pi}\left(\frac{f^*}{\mu}\right)^2 \frac{m}{\sqrt{s}}\,|\vec{p}_{cm}|^2\,\theta\left(\sqrt{s} - m - \mu\right) \tag{B.31}$$

For the $N^*(1440)$ and $N^*(1520)$ we take the same formula (B.30) changing the width. For the $N^*(1440)$ we take

$$\Gamma_{N^*}(s) = \Gamma_{N^*}(s = m_{N^*}) \frac{q^3_{cm}(s)}{q^3_{cm}(m_{N^*})} \tag{B.32}$$

while for the $N^*(1520)$ we take

$$\Gamma_{N'^*}(s) = \Gamma_{N'^*}(s = m_{N'^*}) \frac{q^5_{cm}(s)}{q^5_{cm}(m_{N'^*})} \tag{B.33}$$

assuming in both cases that the energy dependence is given by the decay of the resonance in $N\pi$ and that they are respectively P wave and D wave resonances.

The π and ρ propagators are given by

$$D_\pi(q) = \frac{1}{q^2 - \mu^2 + i\epsilon} \tag{B.34}$$

$$D_\rho(q) = \frac{1}{q^2 - m^2_\rho + i\omega(\vec{q})\Gamma_\rho(s)} \tag{B.35}$$

with

$$s = p^{0\,2} - \vec{p}^{\,2} \quad ; \quad \omega(\vec{q}) = \sqrt{m^2_\rho + \vec{p}^{\,2}}$$

$$\Gamma_\rho(s) = \frac{2}{3} \frac{f^2_\rho}{4\pi} \frac{1}{s} |\vec{p}_{cm}|^3 \tag{B.36}$$

For the off shell pions and ρ-mesons we use form factor in the vertices of the monopole type

$$F(q) = \frac{\Lambda^2 - m^2}{\Lambda^2 - q^2} \quad ; \quad \Lambda \simeq 1.3\ GeV \tag{B.37}$$

In all formulae we have assumed that $\sigma^i \equiv \sigma_i$, $S^i \equiv S_i$, $T^i \equiv T_i$ are euclidean vectors. However ∂_i, A_i, $\vec{\phi}^{(\rho)}_i$, p_i, etc., we have respected their covariant meaning.

References

[1] Aachen-Berlin-Bonn-Hamburg-Heidelberg-München collaboration, Phys. Rev. **175** (1968) 1669.

[2] G. Gianella et al., Nuovo Cimento **LXIII A** (1969) 892

[3] G. Tamas et al., private communication.

[4] L. Lüke and P. Söding, Springer Tracts in Modern Physics **59** (1971) 39.

[5] C. W. Bjork et al., Phys. Rev. Lett. **44** (1980) 62.

[6] M. E. Sevior et al., Phys. Rev. Lett. **66** (1991) 2569.

[7] A. Rahav et al., Phys. Rev. Lett. **66** (1991) 1279.

[8] R. A. Arndt et al., Phys. Rev. **D20** (1979) 651.

[9] R. S. Bhalerao and L. C. Lin, Phys. Rev. **C30** (1984) 224.

[10] E. Oset and M.J. Vicente-Vacas, Nucl. Phys. **A446** (1985) 584.

[11] O. Jäkel et al., Nucl. Phys. **A511** (1990) 733.

[12] V. Sossi et al., Nucl. Phys. **A548** (1992) 562.

[13] V. Sossi, N. Fazel, R. R. Johnson and M. J. Vicente-Vacas, Phys. Lett. **B298** (1993) 287.

[14] J. Gasser and H. Leutwyler, Ann. Phys. (NY) **158** (1984) 142.

[15] E. Oset and M. J. Vicente-Vacas, in Int. Symposium on weak and electromagnetic interactions in nuclei, Heidelberg, 1986, H. K. Klapdor Ed., Springer-Verlag, pag 444.

[16] E. Oset and M. J. Vicente-Vacas, Nucl. Phys. **A454** (1986) 637.

[17] N. Grion et al., Nucl. Phys. **A492** (1989) 509.

[18] T.E.O. Ericson and W. Weise., Pions and nuclei, Clarendon Press, 1988

[19] R. C. Carrasco and E. Oset, Nucl. Phys. **A536** (1992) 445.

[20] T. D. Cohen, Phys. Lett. **233** (1989) 467.

[21] J. A. Gómez-Tejedor, Tesina de Licenciatura, Universidad de Valencia, 1993.

[22] J. Koch, E.J. Moniz and N. Ohtsuka, Ann. Phys. 154 (1984) 99.

[23] M. B. Johnson, E. R. Siciliano, H. Toki and A. Wirzba, Phys. Rev. Lett. **52** (1984) 593.

[24] J. D. Bjorken and S. D. Drell, Relativistic Quantum Fields, Mc Graw-Hill, New York 1965.

[25] Particle Data Group, Phys. Rev. **D45** (1992).

[26] F. E. Close, An introduction to quarks and partons, Ed. Academic Press, London, 1979.

[27] A. Bosshard et al., Phys. Rev. **D44** (1991) 1962.

[28] Review of Particle Properties, Rev. Mod. Phys. **56** (1984)

[29] S. L. Adler, Phys. Rev. **177** (1969) 2426.

[30] J. Bell and R. Jackiw, Nuovo Cimento **60A** (1971) 95.

[31] L. Heller, S. Kumano, J. C. Martínez and E. J. Moniz, Phys. Rev. **C35** (1987) 718.

[32] R.D. Amado, Modern Three-Hadron Physics, Ed. A.W. Thomas, Springer-Verlag, 1977

[33] M.G. Olson, Nucl. Phys. **B78** (1974) 55.